IRANIAN JOURNAL OF CATALYSIS

Synthesis and Catalytic Performance of Ni/Silica Pillared Clay on HDPE Plastic Hydrocracking to Produce Liquid Hydrocarbons as Fuel

Darwanta Darwanta[a,b], Wega Trisunaryanti[a,*], Karna Wijaya[a], Suryo Purwono[c]

a)Department of Chemistry, Faculty of Mathematics and Natural Sciences, Gadjah Mada University, Yogyakarta, Indonesia

b)Department of Chemistry, Faculty of Mathematics and Natural Sciences, Cenderawasih University, Jayapura, Indonesia

c) Department of Chemical Engineering, Faculty of Engineering, Gadjah Mada University, Yogyakarta, Indonesia

Received 6 February 2023; received in revised form 16 June 2023; accepted 29 June 2023 (**DOI: 10.30495/IJC.2023.1979198.1992**)

ABSTRACT

Synthesis of Ni/SiPILC (Silica Pillared Clay) catalyst based on light fraction clay for hydrocracking of High-density Polyethylene (HDPE) plastics into liquid fuels has been carried out. The SiPILC was synthesized using CTAB and TEOS by varying the TEOS/clay mole ratio. The Ni metal was impregnated on the SiPILC with a variation of 2, 4, 6, and 8 wt% of Ni. Hydrocracking of HDPE plastic was carried out using catalysts in a semi-batch stainless steel reactor. The liquid cracking product was analyzed using GC-MS. The results showed that the clay consisted of Montmorillonite, Cristoballite, and Quartz minerals. The highest specific surface area of 571 m^2/g was showed by the SiPILC treated by TEOS/clay mole ratio of 60. Ni 2%/SiPILC achieved the best performance catalyst with the highest acidity of 1.327 mmol/g that produced a liquid fraction of 45.50% (gasoline 55.03 % and diesel 44.96 %) at hydrocracking temperature 450 ^oC for 1.5 h. The Ni 2% /SiPILC catalyst still performed well after the fifth hydrocracking run, producing a liquid fraction of 41.08 %.

***Keywords**: Silica-pillared clay; Ni/SiPILC catalyst, hydrocracking, HDPE plastic waste*

1. Introduction

The need for plastic has grown rapidly in the last 20 years, with a growth rate of ~5%/year, causing several problems related to waste management [1]. Globally production of plastic polymers has reached 368 million tonnes in 2021. Plastic production has increased more than 20 times over the last 50 years, and if this pattern persists, it is estimated that plastic production will exceed 500 million tonnes by 2050 [2] [3]. In 2020, 29 million tonnes of plastic waste accumulated in Europe, of which 23.4% have been disposed of in landfills [4]. Plastic production includes 32% polyethylene, 20% polypropylene, and 17% polyvinyl chloride [5]. HDPE plastic is a type of plastic used for industry, especially packaging, and construction [6]. Plastic waste is a difficult material to decompose biologically, so its presence in the environment can reach hundreds of years, causing it to pollute the environment [7].

*Corresponding author:
E-mail address: wegats@ugm.ac.id (**W. Trisunaryanti**)

In European Union, the distribution of plastic waste management is 24.9% is landfill, 32.5% is recycled, and 42.6% is processed into an energy source [8]. Plastic waste management in developing countries, including Indonesia, is far worse than in developed countries like the European Union. It is caused by many factors, such as the government's low commitment to plastic waste management policies, low public awareness to adopt a clean lifestyle, and the undeveloped technology for processing waste, including plastic waste, into valuable materials on a large scale.

HDPE plastic contains 99.81% volatile matter and 0.18% ash, so it has the potential to be processed into liquid and gas products with minimal solid residue [5]. One of the processing of plastic waste that has recently been developed is the processing of plastic waste into alternative energy such as liquid fuel. Conventional pyrolysis/thermal decomposition process plastic waste into oil, solid residue (char), and gas at temperatures of 300-900°C. The limitation of pyrolysis is that the whole process is highly dependent on temperature [9], and the

resulting liquid oil still contains residues [10]. So, it is necessary to develop a catalyzed cracking process. Using catalysts can increase the degradation reaction at lower temperatures to save energy [11]. Catalyzed degradation can improve product selectivity and produce high-quality liquid fuels.

So far, the catalysts widely used for HDPE degradation are solid acids such as zeolites, filter molecules, and silica-alumina [6]. The limitations of the zeolite-based catalyst for plastic cracking are the limited pore size (maximum 8 Å) and the acidity, which is too high, which results in the product being dominated by gas [12]. Although the price is relatively low, the use of clay for cracking catalysts is hampered by the small pore size of the clay (micropores) and low heat resistance, which makes it easily damaged for high-temperature applications. Catalyst modification has overcome this limitation, and it is necessary to modify it so that clay can be used as an alternative catalyst. Currently, pillared silica clay-based catalysts have been developed.

The intercalation process can change the clay structure to pillared clay. Silica pillared clay (SiPILC) is the most attractive type, with hydrophobic properties and high heat resistance [13] for various applications. SiPILC, which has a large specific surface area, strongly supports its use as a metal catalyst solid support. SiPILCs with relatively specific surface areas of 482 m^2/g [13], 712.4 m^2/g [14], and 1874 m^2/g [15] were successfully synthesized. SiPILC's good thermal resistance strongly supports its use as a catalyst involving relatively high temperatures, such as cracking. The good thermal resistance of SiPILC has been widely reported, including 800°C [16], 750 °C [17], and 600 °C [18].

Nickel metal has been widely used as a catalyst in the cracking industry, including cracking plastic waste. Ni metal is often spread on suitable solid supports to improve its catalytic performance. Sriningsih *et al.* [19] synthesized Ni/natural zeolite and used it as a catalyst for the cracking process of LDPE (Low-Density Poly Ethylene) plastic waste to produce liquid fuel. The cracking process was carried out at 450°C for 1 hour to produce 30.64% liquid, 68.27% gas, and 1.10% solid (coke). Yao *et al.* [20] synthesized Ni/Al_2O_3 as a catalyst to process Poly Styrene (PS) type plastics to produce syngas containing 62.26 mmol H_2/g plastic and 36.10 mmol CO/g plastic. Qureshi *et al*. [21] synthesized a natural 10% Ni-clay impregnation catalyst used for the cracking process of LDPE plastic and used plastic bags at a temperature of 350°C with a liquid yield of 79.23% for LDPE and 76.01 % for used plastic bags. Ni impregnation has increased the liquid product by 12% for LDPE and 18.6% for used plastic bags. Liquid products have the character of liquid fuels in the range of gasoline, kerosene, and diesel oil. Meanwhile, Al-asadi and Miskolczi [22] synthesized Ni/zeolite, used it as a catalyst in the cracking process of Polyethylene terephthalate (PET) plastic, and succeeded in increasing the cracking yield. Mangesh *et al.* [23] synthesized Ni/ZSM-5 and used it as a catalyst for the hydrogenation of oil from polypropylene plastic pyrolysis at a pressure of 70 bar and a temperature of 350°C. The resulting oil has chemical properties similar to EN590 standard fuel. However, no one has reported using Nickel metal in silica-pillared clays as a catalyst for hydrocracking HDPE plastics. The success of this related research is significant for the development of processing a lot of HDPE plastic waste into alternative liquid fuels.

2. Experimental

2.1. Materials and equipment

The materials used in this study were commercial clay with Bentonite trademark in petshop usually for the maintenance of cats. Cetyl Trimethyl Ammonium Bromide (CTAB), Tetra Ethyl Ortho Silicate (TEOS) purchased from Sigma-Aldrich, $Ni(NO_3)_2.6H_2O$, ethanol, universal pH paper, pyridine from Merck and distilled water. The equipment used includes an X-ray diffractometer (X'pert PRO, PANalytical) with CuKα radiation (λ= 0.154 nm), Gas Sorption Analyzer brand Gemini VII 2390, GC-MS Merck Shimadzu GC2010, Spectrophotometer FTIR prestige 21 Shimadzu, Scanning JEOL JSM-6510LA Electron Microscope (SEM), PERKIN ELMER 3110 Atomic Absorption Spectrophotometer.

2.2. SiPILC and Ni/SiPILC preparation

20 g of clay was dispersed in 300 mL of distilled water, stirred with a magnetic stirrer at 400 rpm for 3 hours, and let stand for 12 hours to form precipitate and suspension—separation of precipitate as a heavy fraction and suspension as light clay fraction. As much as 4 g of light fraction clay was dispersed in 70 mL of distilled water and stirred with a magnetic stirrer for 3 hours at a rotational speed of 400 rpm to form a suspension. As much as 4 g of CTAB was dissolved in 10 mL of ethanol and added dropwise into the clay suspension accompanied by stirring, and the pH was adjusted to 2 by adding 1 M HCl solution dropwise. TEOS is added 1mL/min into the suspension according to variations in the TEOS/clay mole ratio: 10; 20; 40; 60, and 80, then stirred for 12 hours at room temperature. The mixture was then put into the autoclave reactor and heated in an oven at 110°C for 24

hours. The mixture was then dried in an oven at 110ºC for 5 hours, crushed, and sieved through 100 mesh. The dried solid was then calcined at 500ºC for 4 hours with a flow of N_2 gas at a speed of 20 mL/min, and the result was called SiPILC.

Impregnation of Ni metal on SiPILC refers to the method of Sriningsih *et al.* [19]. $Ni(NO_3)_2.6H_2O$ was dissolved in 100 mL of distilled water with various weights, namely 1; 2, 4; 6; 8% (w/w) of 10 g SiPILC. The mixture was refluxed at 90 °C for 4 hours, then filtered and dried in the oven at 110 ºC for 3 hours. The solid obtained was heated in a 450-watt microwave for 30 minutes at 90ºC. Furthermore, the solids were reduced by calcination at 400°C for 3 hours with a flow of H_2 gas at a flow rate of 20 mL/minute to obtain a Ni/SiPILC catalyst.

2.3. Characterization

Initial clay, light fraction, heavy fraction, SiPILC, and Ni/SiPILC were characterized by XRD at a measurement angle of 2θ =3-60°. The ammonium acetate method measured the initial clay cation exchange capacities and light fractions: a Gas Sorption Analyzer analyzed surface area, pore volume, and average pore size. The catalyst acidity test was carried out using the pyridine gas absorption gravimetric method followed by FTIR characterization in the 4000-400 cm^{-1} wave number region. Scanning Electron Microscope (SEM) analyzed the material's surface morphology.

2.4. The catalytic performance in HDPE plastic hydrocracking

Using a semi-batch reactor, the synthesized catalyst was tested for its catalytic activity in the HDPE plastic hydrocracking process (**Fig. 1**). The hydrocracking process was carried out at 450 °C for 2 hours with an H_2 gas flow rate of 20 mL/minute. The weight ratio of HDPE plastic to catalyst is 5. The hydrocracking liquid product is isolated by cooling ice sprinkled with salt. The salt used is commercial sea salt with the main content of NaCl. Further studies were carried out at temperatures of 450 °C, 475 °C, and 500 °C, and time optimization was carried out (variations: 0.5; 1, 1.5, and 2 hours). Reusability was studied on the catalyst with the best performance by reusing the catalyst with a new HDPE plastic feed for five repetitions.

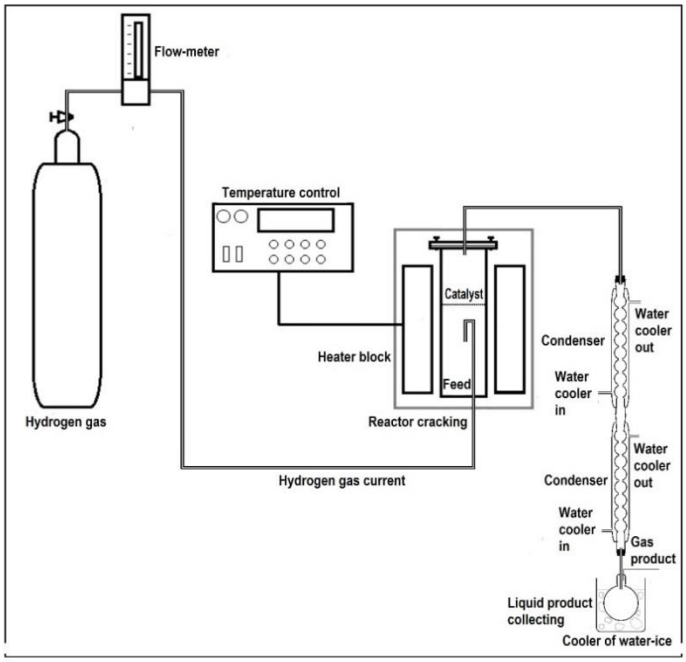

Fig. 1. Design of HDPE plastic hydrocracking semi-batch reactor

2.5. Analysis of HDPE plastic hydrocracking products

Calculating product composition hydrocracking refers to Ghaffar *et al.* [24] with calculations using equations 1-5. Weight of the liquid product (W_l,g), Weight of residual solids/coke (Ws,g), Weight of feed HDPE plastic (W_f,g), liquid product fraction (F_l, %), solid product fraction (Fs, %), gas product fraction (Fg, %) and total conversion (Tc, %), selectivity for the formation of liquid products (S_l, %). Liquid products were characterized using GC-MS.

$$F_l\,(\%) = \frac{Wl}{Wf} \times 100\% \quad \text{.....(1)}$$

$$F_s\,(\%) = \frac{W_s}{W_f} \times 100\% \quad \text{.....(2)}$$

$$F_g\,(\%) = \frac{W_f - (W_l + W_s)}{Wf} \times 100\% \quad \text{.....(3)}$$

$$Tc\,(\%) = \frac{Fl + Fg}{Wf} \times 100\% \quad \text{.....(4)}$$

$$S_l\,(\%) = \frac{Fl}{Tc} \times 100\% \quad \text{.....(5)}$$

3. Results and Discussion

3.1. Clay structure and phase

Separation of the initial clay fraction resulted in a light fraction of 41.83% and a heavy fraction of 58.17%. The results of the XRD characterization of the initial clay, light, and heavy fractions were compared with standard mineral data (rruff.info: R110052 (Montmorillonite),

R061107 (Cristobalite), R110108 (Quartz)) as shown in **Fig. 2**.

Based on the data in **Fig. 2** and the conformity of the prominent peaks of the standard minerals, information was obtained that the initial clay contained Montmorillonite, Cristoballite, and Quartz. The separation process has increased the peak intensity of Montmorillonite and Cristoballite minerals and conversely decreased the peak intensity of Quartz minerals for the clay light fraction. In the clay-heavy fraction, the opposite occurred, where there was a decrease in the peak intensity of Montmorillonite and Cristoballite and an increase in the peak intensity of Quartz minerals. Quartz minerals contain the main composition SiO_2, which has a very stable crystal structure, cannot expand (swelling), and has a relatively more significant specific gravity, making it relatively easier to precipitate as a heavy fraction. The results of the XRF analysis showed that the relative SiO_2 content in the initial clay was 87.54%, which was then separated into 83.57% in the heavy fraction and 28.67% in the light fraction. These results confirm the previous XRD data that the Quartz peak is dominant in the early clay and heavy fractions but can still be detected in the light fraction. The presence of Montmorillonite and Quartz minerals in the clay agrees with the report of Geramian *et al.* [25] and Barakan and Aghazadeh [26]. The decrease in the mineral content of Quartz and the increase in the intensity of Montmorillonite in the clay light fraction indicates that the amorphous SiO_2 composition can be rearranged through the synthesis process to become pillared clay.

Furthermore, the material characterization of the results of clay separation was carried out by SEM, shown in **Fig. 3**. Based on **Fig. 3**, the results of the SEM images show that the initial clay samples appear to have clumps covered with delicate layers that are still mixed. These fine layers as arranged sheets characterize clay materials with a layered structure. The delicate layers increased in number and were more uniform in the light fraction (**Fig. 3B**) than the initial clay. SEM results of clay in irregular fine sheets were also reported [15, 27, 28]. The process of dispersion of clay in distilled water accompanied by stirring is thought to cause the peeling of the fine layer that covers shapes with a specific shape. It is proven by the SEM image **Fig. 3(C)** for the heavy fraction. It is seen that there are more and more shapes with more precise field boundaries and more apparent shapes. These structures show a material with better crystallinity, and when correlated with the previous XRD data, it is estimated as the mineral Quartz (2θ = 26.6°).

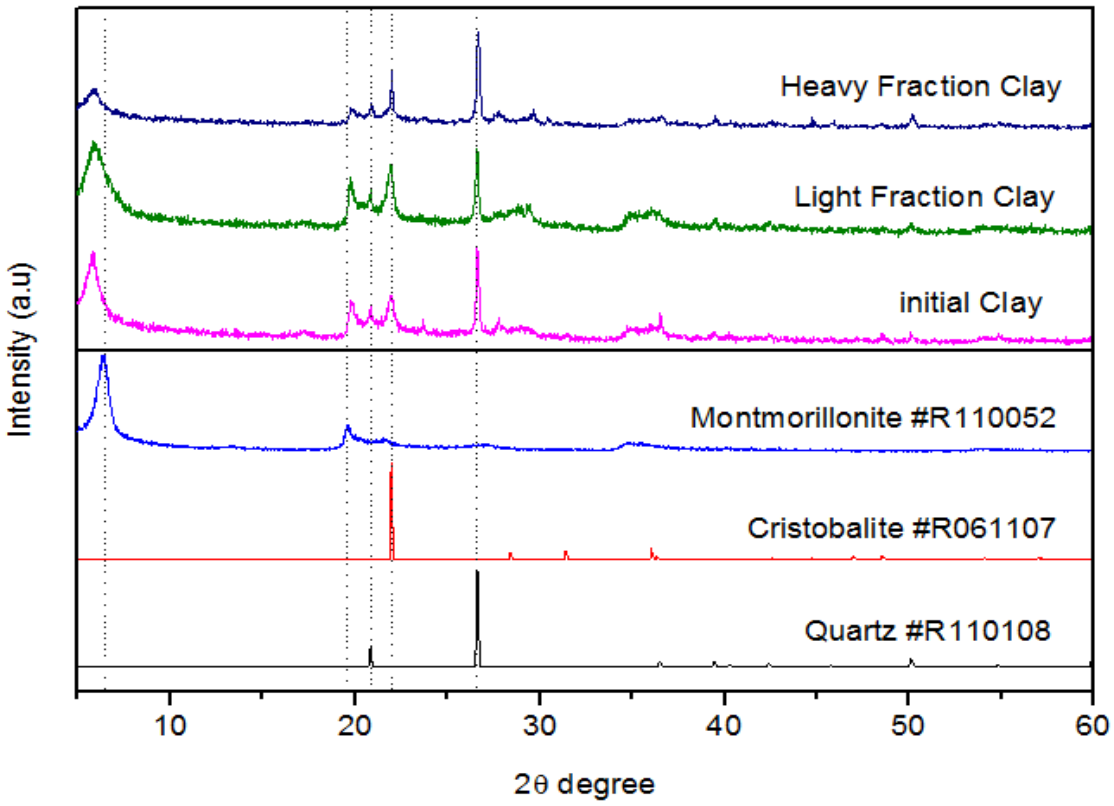

Fig. 2. Diffractogram of the initial clay, light, and heavy fractions of clays and standard minerals. M = Montmorillonite, C = Cristoballite, Q = Quartz

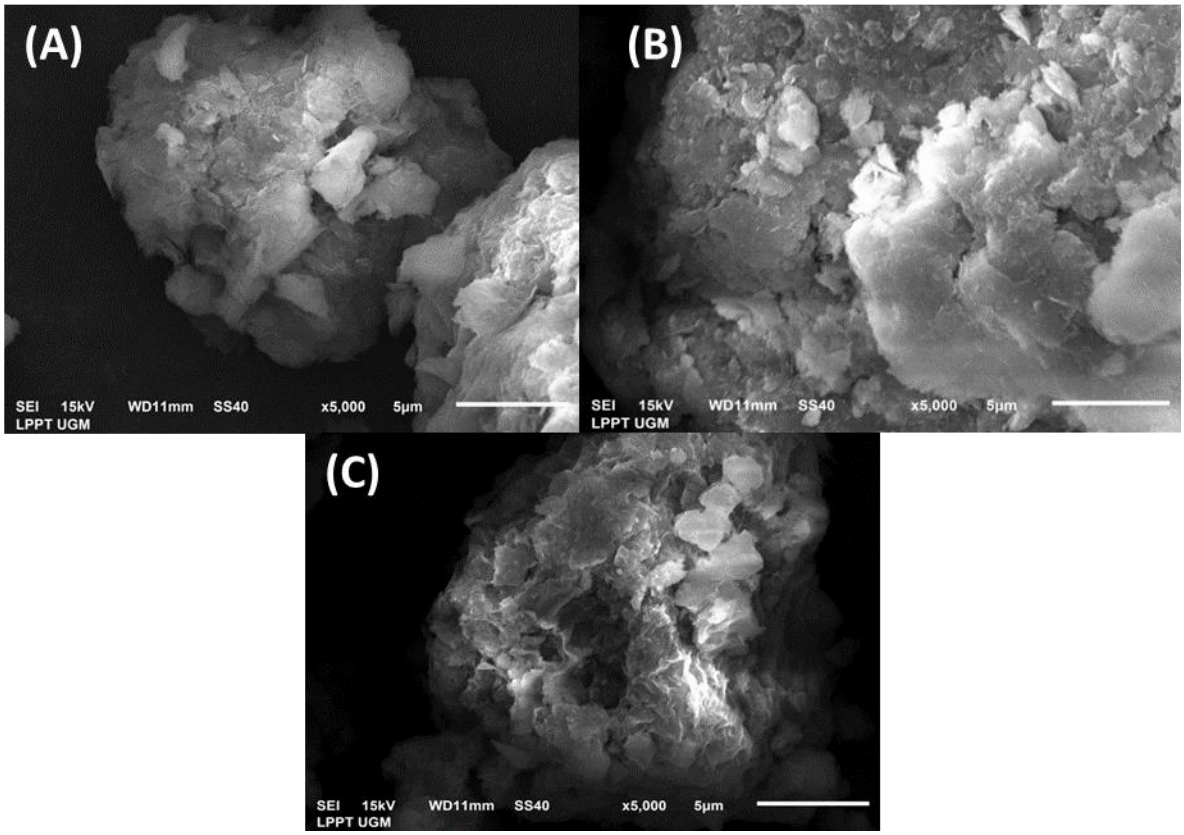

Fig. 3. SEM images of the initial clay (A), the clay light fraction (B), and the clay-heavy fraction (C), with a magnification of 5000 times

Measurement of the value of Cation Exchange Capacity (CEC) obtained 49 meq/100 g for the initial clay and increased to 54.50 meq/100 g for the clay light fraction. The separation process was also proven to increase the value of CEC, although relatively small, at 11.22%. Increasing the CEC value of the light fraction supports the pillaring process in the following pillared clay synthesis, where the synthesis process begins with the insertion of CTA^+ surfactant molecule ions (Cetyltrimethylammonium) to replace ions between layers of clay with cation exchange phenomena. Several researchers reported using clay to synthesize SiPILC with different CECs, for example, 91 meq/100 g [29] and 92.6 meq/100 g [30]. The CEC value of the light fraction of the clay used has a relatively lower value than other researchers' data. It is possible because many factors can affect the CEC value of clay, for example, the process of forming clay minerals in their natural environment.

3.2. Synthesis of SiPILC

SiPILC synthesis uses clay light fraction as base material with CTAB as a guide (template) and TEOS silica as a source of TEOS/clay mole ratio study: 10; 20; 40; 60, and 80. The XRD results of the synthesized SiPILC are shown in **Fig. 4** and **Table 1**.

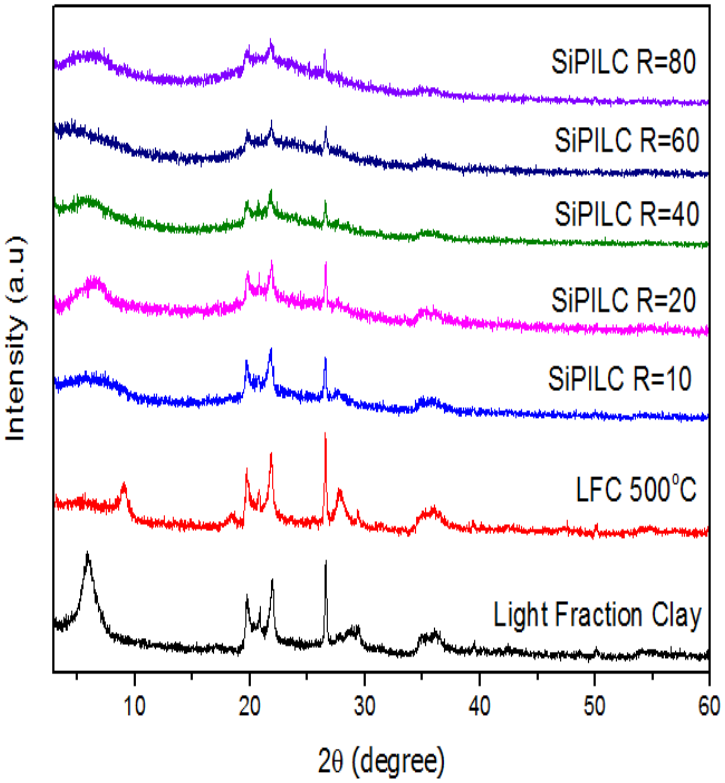

Fig. 4. Diffractogram of a clay light fraction, light fraction calcined at 500°C, SiPILC with variations in the ratio (R) mol TEOS/clay = 10; 20; 40; 60 and 80

Table 1. Angle 2θ of peak d_{001} from a clay light fraction, a light fraction of calcined clay at 500°C and SiPILC with variations in the TEOS/clay mole ratio

Sample	Angle of 2θ (°)
Light Faction	5.849
Light Fraction 500°C	9.024
R=10	5.682
R=20	4.412
R=40	5.030
R=60	3.075
R=80	3.075

Based on the diffractogram in **Fig. 4** and **Table 1**, the tilting phenomenon of the clay structure is indicated by the detection of the d_{001} peak of Montmorillonite in the area around the corner 2θ = 3.075-5.682° for SiPILC. The d_{001} peak has a low intensity and tends to widen. The same phenomenon was also reported [13, 14, 31]. The data in **Table 1** shows that the greater the TEOS/clay mole ratio, the d_{001} peak shifts towards the slight 2θ angle. It means that the more TEOS as a source of SiO_2, the more pillars will be formed. One measure of the success of pillaring the clay structure with silica pillars can be seen from how much the d_{001} peak shifts to the left (to a slight 2θ angle), which indicates a widening of the space between the clay layers due to the formation of supporting pillars. Based on **Table 1** data, it can be seen that the peak d_{001} shifts to the left at maximum at R = 60, reaching 3.075°. The opposite phenomenon for the light fraction without silica pillars, where heating at 500°C has caused the d_{001} peak to shift to the right to an angle of 2θ = 9.024° with decreasing intensity. It indicates that the heating of 500°C for 4 hours indicates that the clay structure has begun to collapse due to heating. The result of calculating the d-spacing of the synthesized SiPILC is shown in **Fig. 5**. The higher the TEOS/clay mole ratio, the space between the clay layers tends to increase and reaches an optimum at R=60.

Further characterization was carried out using a Gas Sorption Analyzer, shown in **Fig. 6**, to prove the successful pillaring of clay structures with silica pillars.

Based on **Fig. 6**, it can be seen that the adsorption-desorption curve of the N_2 isotherm concerning relative pressure (P/P°) for the clay light fraction and SiPILC produced by the synthesis forms a sloping curve at low relative pressure indicating the formation of a monolayer on the light fraction surface and SiPILC. At relatively higher pressures, multilayers begin to form, with graphs starting to form loops where N_2 gas begins to occupy the space between the layers of the material. The characteristics of the adsorption-desorption isotherm correspond to the type IV isotherm graph, which states the type of adsorption on the mesoporous surface. In general, silica stretching in the clay light fraction is evident that the greater the TEOS/clay mole ratio has increased the quantity of N_2 gas absorbed, which results in more open pore stretching, making it more possible for more N_2 gas as an absorbent to be absorbed. It is evidenced by the widening of the absorption-desorption curve so that the hysteresis area also increases. This phenomenon indicates a process of growing the number of pillars which increases with the increasing number of TEOS used. Furthermore, other parameters obtained from the GSA characterization are the pore distribution for the increase in the pore volume of the clay light fraction, and SiPILC synthesized, as shown in **Fig. 7**.

Based on **Fig. 7**, it can be seen that the light fraction is a porous material with a pore size dominated at 4 nm. Silica pillaring in the clay structure has been shown to open up the space between the clay layers, thereby increasing the dominant pore size with a more than 12 nm diameter. The data is corroborated with other parameters from the GSA characterization results, shown in **Table 2.**

Based on the data in **Table 2**, it can be seen that the light fraction of the clay used is a porous material with a specific surface area of 77.90 m^2/g and a pore volume of 0.213 cm^3/g. One of the weaknesses of clay material for cracking catalyst applications is its low thermal resistance. It is evidenced by heating at 500°C for 4 hours, which decreased the specific surface area to 30.4 7 m^2/g and pore volume of 0.162 cm^3/g so that the clay does not have the property of swelling again and losing porosity. This data agrees with the previous XRD data (**Fig. 4** and **Table 1**).

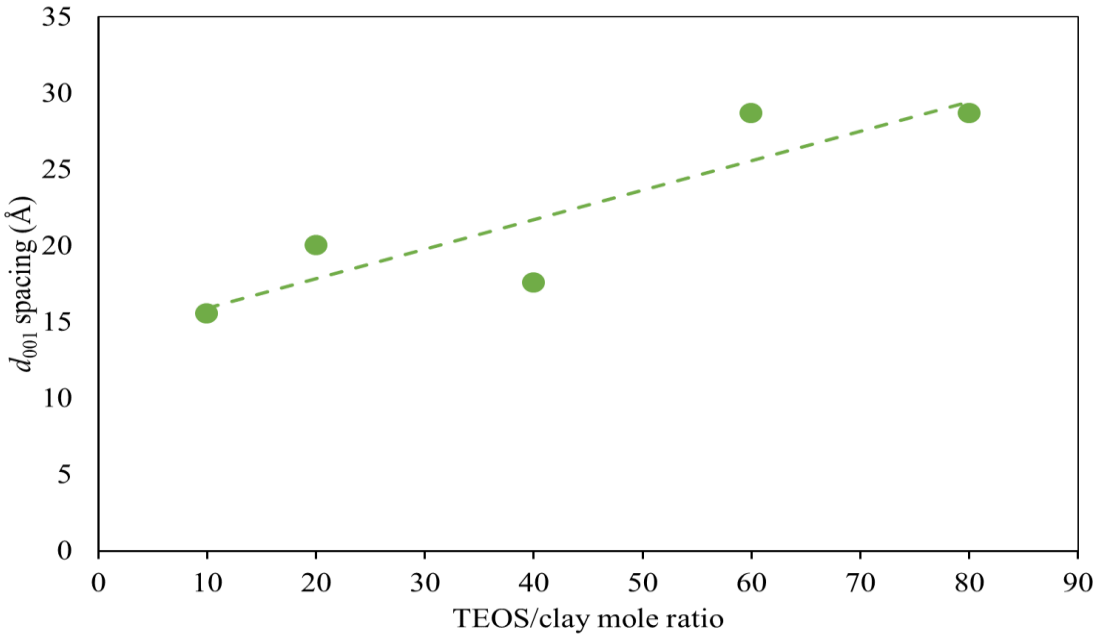

Fig. 5. The size of the SiPILC d-spacing relative to variations in the TEOS/clay mole ratio

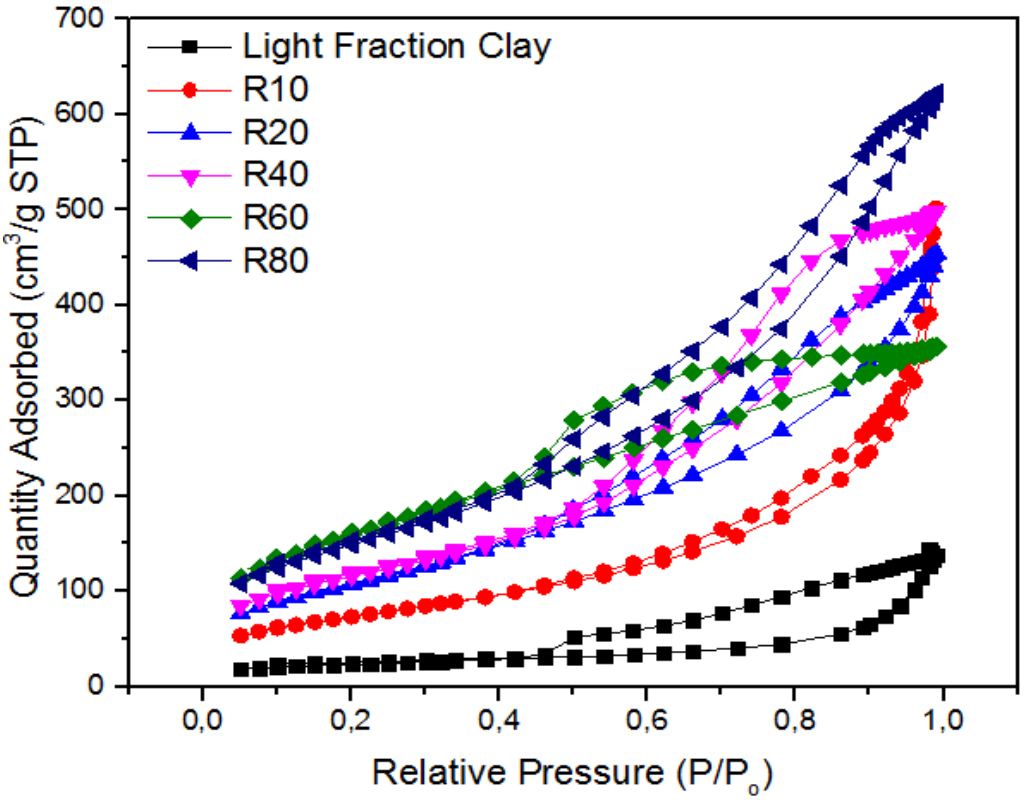

Fig. 6. Absorption-desorption hysteresis pattern of a clay light fraction and SiPILC with a variation of TEOS/clay mole ratio: 10; 20;40; 60 and 80

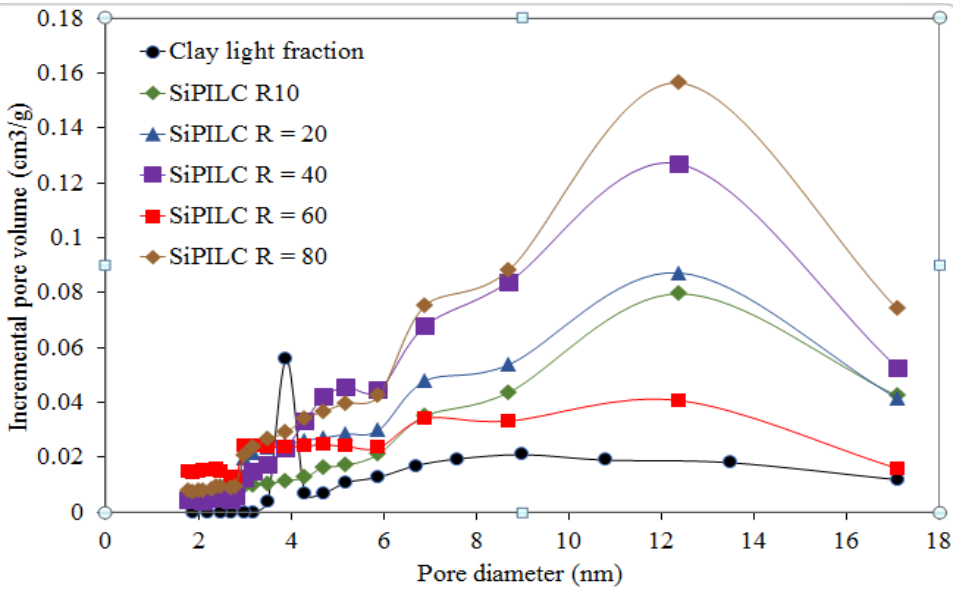

Fig. 7. The pore distribution of the clay light fraction and SiPILC with variations in TEOS/clay mole ratios

Table 2. Specific surface area, pore volume, and the average pore diameter of the light fraction, the light fraction of calcined clay 500°C and the synthesized SiPILC

Sample	Specific Surface Area (m^2/g)	Pore Volume (cm^3/g)	Average pore diameter(nm)
Light Fraction	77.90	0.213	10.913
Light Fraction 500°C	30.47	0.162	21.119
SiPILC R=10	263.36	0.763	11.593
SiPILC R=20	395.58	0.698	7.058
SiPILC R=40	412.43	0.771	7.475
SiPILC R=60	570.66	0.551	3.862
SiPILC R=80	535.50	0.960	7.171

The opposite phenomenon occurs for SiPILC, where the increased specific surface area evidences the successful pillaring of clay structures with silica pillars and pore volume of all synthesized SiPILCs compared to the clay light fraction. This results from loosening the space between the clay layers and the formed silica pillars. From the results of the TEOS/clay mole ratio study, it can be seen that the TEOS/clay mole ratio is 10-60 showed a consistent increase in specific surface area and reached a maximum at a ratio of 60, which reached 570.6 6 m^2/g. It supports previous data that there is a growth in silica pillars formed with the increasing use of silica sources. Forming the maximum number of pillars allows new pore systems in the interlayer clay spaces. It is evidenced by the average diameter, which tends to decrease with increasing TEOS/clay mole ratio. However, the specific surface area decreased at the TEOS/clay mole ratio 80, indicating that the optimum variation had been exceeded. At a ratio of 80, it is likely due to the abundance of resources. Silica partially forms too large polymers, so some have difficulty entering the pores between the clay layers. The success of silica pillaring with evidence of an increase in specific surface area with different results, for example, 1006 m^2/g [27], 712.4 m^2/g [14], 482 m^2/g [13]. The difference in specific surface area values between the results of this study and various research reports is very likely due to many factors that can affect the quality of the resulting SiPILC, for example, the type and properties of the initial clay used, the method of pillaring, the type of surfactant used. Based on the XRD and GSA data, SiPILC was chosen with a TEOS/clay = 60-mole ratio as the best ratio for further research. A comparison of the SEM results of the clay light fraction with SiPILC R=60 is given in **Fig. 8**.

Morphological comparison of the light fraction and SiPILC R = 60 were characterized by SEM, whose results are presented in **Fig. 8**. The SEM image of the clay light fraction looks like a cloud of fog. The flakes are not uniform with a random arrangement. Meanwhile, the SEM images for SiPILC appear to be more expanded and relatively more uniform due to the phenomenon of pillaring of the space between the clay layers and the silica pillars. This display depicts material that has not been damaged even though it has passed the

calcination stage at 500°C for 4 hours. SEM results that expand from SiPILC compared to the initial clay were also reported [14]. The relatively high thermal resistance properties and large specific surface area make SiPILC a material. It is potentially a metal-supporting solid for catalysts, especially when it involves relatively high temperatures, such as the hydrocracking process. The development of Ni metal catalyst by impregnation method was characterized by XRD, the results of which are shown in **Fig. 9**.

Based on **Fig. 9**, Ni/SiPILC compared to SiPILC does not provide a very significant difference. Even variations of the addition of Ni impregnated on SiPILC also did not give any difference in the peaks. A slight difference between SiPILC and Ni/SiPILC is only seen at the d_{001} peak, which seems to decrease in intensity. It is probably the effect of 450-watt microwave treatment for 30 minutes and 400°C reduction heat for 3 hours at the impregnation stage. Impregnation of Ni metal from $Ni(CO_3)_2.6H_2O$ solution into solid SiPILC can form NiO and Ni^0. According to Richardson *et al.* [32], the two forms of Ni will be detected by XRD characterization at an angle of 2θ for NiO: 43.29; 37.26 and Ni^0: 44.50; 51.86°.

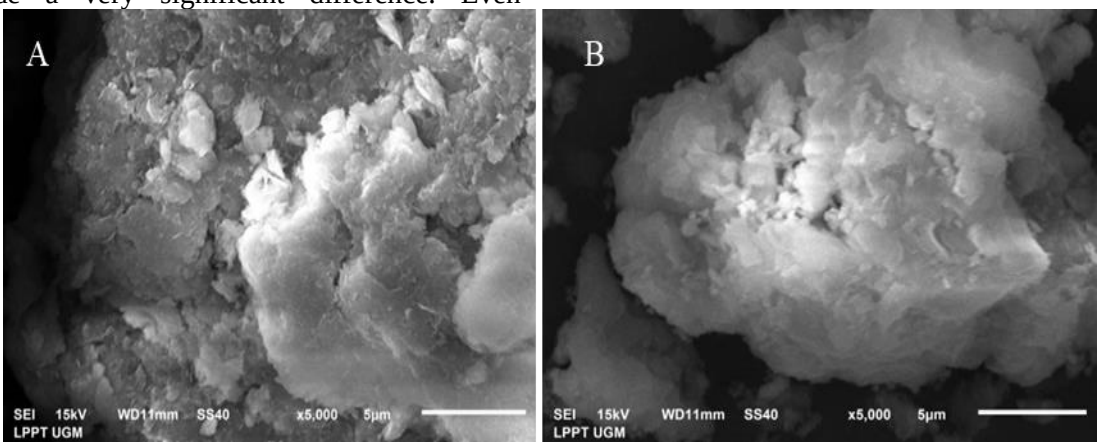

Fig. 8. SEM images of clay light fraction (A) and SiPILC R = 60 (B)

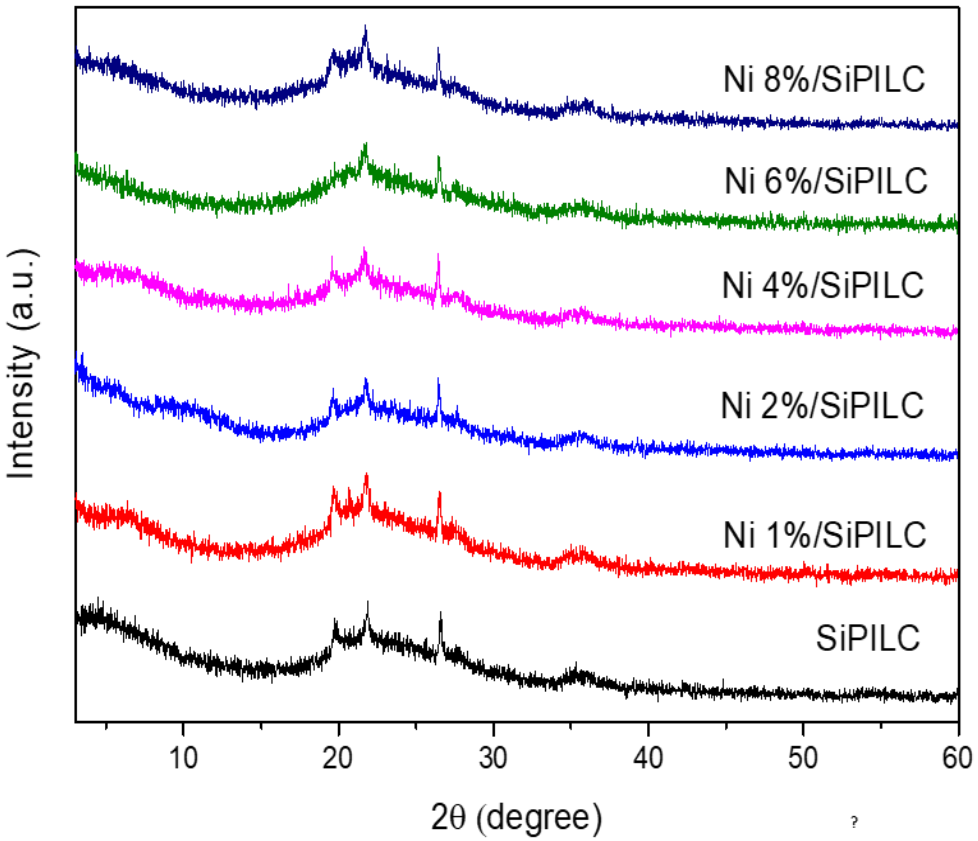

Fig. 9. SiPILC and Ni/SiPILC catalyst diffractograms with the variation of % Ni initially impregnated

Meanwhile, Aguado *et al.* [33] reported that the peak of NiO impregnated in beta zeolite appeared in the region 2θ = 37.2; 43.2 and 62.8°. However, in the diffractogram of **Fig. 9**, these peaks are not visible. It is possible that the amount of Ni that was successfully impregnated on SiPILC was too small. The characteristic green colour of the $Ni(CO_3)_2.6H_2O$ solution, which becomes more concentrated with increasing Ni concentration in the impregnated filtrate, is evidence that not all Ni was successfully impregnated in SiPILC. However, the successful impregnation of Ni metal in the SiPILC structure can still be proven from atomic absorption spectrophotometric analysis for Ni metal in **Table 3**.

Based on the data in **Table 3**, it can be seen that all solids after impregnation have a Ni content greater than SiPILC. It proves that Ni metal has been successfully included in the SiPILC structure. In addition, an increase in the percentage of Ni also tends to increase the impregnated Ni content. However, the considerable increase in the percentage of impregnated Ni was not followed by a considerable increase in the successfully impregnated Ni. For example, Ni 2%/SiPILC to Ni 8%/SiPILC increased by 300% but only resulted in a 47% increase in impregnated Ni. The Ni 2%/SiPILC variation is the best for the efficient use of chemicals. Although very little Ni was also detected for SiPILC, it is possible that it contained Ni from the original clay used.

A solid catalyst's acidity can be determined by measuring the adsorption capacity of strong base molecules, such as NH_3 and pyridine, carried out gravimetrically [34]. Pyridine and NH_3 molecules have a lone pair of electrons that can play the role of a Lewis base on the acid side of the catalyst so that the number of pyridine or NH_3 moles can indicate the acidity of a solid catalyst. The results of acidity measurements of the clay light fraction, SiPILC, and Ni/SiPILC synthesized results are shown in **Table 4**.

Based on the acidity data from **Table 4**, it can be seen that the acidity of the clay light fraction is still minimal (0.050 mmol/g). The acidity of SiPILC increases significantly to 1.104 mmol/g (an increase of 22 times). It is due to the formation of SiO_2 pillars in the space between the clay layers. Adding Ni metal to SiPILC did not increase the acidity with a consistent pattern. At the variation of Ni 2%/SiPILC, the acidity reaches a maximum. A concentration of 2% may be the best concentration to incorporate Ni metal into the SiPILC structure. The significant increase in acidity from 1.104 mmol/g (SiPILC) to 1.327 mmol/g (Ni 2%/SiPILC) proved that adding Ni metal increased the acid sites. Ni metal has empty orbitals capable of playing the role of a Lewis acid in interacting with lone pairs of electrons from the Lewis base of pyridine.

Table 3. Content of Ni metal in the synthesized catalyst

SAMPLE	Ni content (mg/g)
SiPILC	4.36
Ni 1%/SiPILC	133.17
Ni 2%/SiPILC	272.15
Ni 4%/SiPILC	193.17
Ni 6%/SiPILC	308.27
Ni 8%/SiPILC	400.49

Table 4. The results of measurements of the acidity of the clay light fraction, SiPILC, and Ni/SiPILC with variations of impregnated Ni

Sample	Total acidity (mmol pyridine/g)
Clay light fraction	0.050
SiPILC R60	1.104
Ni 1%/SiPILC	0.986
Ni 2%/SiPILC	1.327
Ni 4%/SiPILC	1.060
Ni 6%/SiPILC	1.007
Ni 8%/SiPILC	1.277

The interaction of the acid side of the Ni/SiPILC catalyst with pyridine molecules can be characterized using FTIR. According to Jystad *et al.* [35], pyridine molecules are commonly used for molecular examination for FTIR spectroscopy because they have several normal modes, which are very sensitive to Lewis and Bronsted acid sites through heteroatoms of N in the ring. This approach, known as Py-FTIR, concentrates on the four normal modes, which will be identified in the wave number region 1400-1650 cm^{-1}. According to Eleeza *et al.* [33], a typical peak around 1600 cm^{-1} indicates pyridine attachment to unsaturated tetrahedral Al^{3+} cations and supports the presence of Lewis acid sites because the molecular markers show typical Lewis acid interactions via coordinate bonds. The results of the FTIR characterization of pyridine absorption on Ni/SiPILC catalysts are shown in **Fig. 10**.

Based on the data in **Fig. 10**, it can be seen that all solids interacted with pyridine, giving absorption in the wave number region: 3449, 1635, 1042, 471 cm^{-1}, and 1443 cm^{-1}, especially for clay light fractions. Absorption at wave number 1635 cm^{-1} indicates the presence of a Lewis acid site that interacts with the electron pair of pyridine. According to Eleeza *et al.* [35], a typical peak around 1600 cm^{-1} indicates pyridine attachment to unsaturated tetrahedral Al^{3+} cations and supports the presence of a Lewis acid site because the molecular markers show a typical Lewis acid interaction through coordinate bonds.

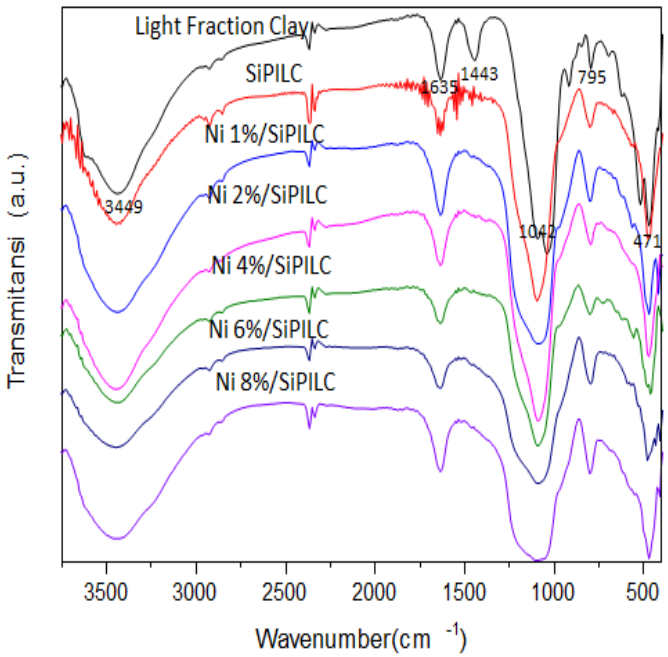

Fig. 10. FTIR spectrogram of pyridine absorption on Ni/SiPILC with a variation of % Ni impregnated on SiPILC

The absorption band at 471 cm^{-1} and 795 cm^{-1} characteristics for Si-O-Si bending vibrations. Meanwhile, the absorption band at 1042 cm^{-1} shows the characteristic absorption of Si-O stretching vibrations in the tetrahedral layer. Sekewael *et al.* [37] reported similar wave number values, which were 470 cm^{-1} and 794 cm^{-1} for Si-O-Si bending vibrations and 1056 cm^{-1} for stretching Si-O in the tetrahedral layer. Absorption at 1443 cm^{-1} for the clay light fraction indicates the presence of Bronsted acid sites, while Sekewael *et al.* [37] reported at 1396 cm^{-1}. According to Garrone and Fajula [34], the species Bronsted acid is shown in the spectrum of the OH stretching region, the location and variation of the absorption band provide information about this. Acid sites on these characterized solids support the acidity data in **Table 4**.

Mao *et al.* [38] stated that the absorption band at 1630 cm^{-1} is associated with Si-OH and higher metal content. Besides that, the precursor metal can also be a strong oxidizing agent, so it oxidizes Si-OH to SiH-O. The solid and wide absorption band at 1000-1200 cm^{-1} is the asymmetric stretching of Si-O in the clay layer. While Sekewael *et al.* [37] stated that the absorption band in the 3441 cm^{-1} area is the –OH stretching vibration of the water molecule, which indicates that all solids absorb water molecules in gaseous form.

3.3. Performance test of Ni/SiPILC catalyst in HDPE plastic hydrocracking process

Ni-impregnated SiPILC with variations: 1; 2; 4; 6, and 8% were then tested for their performance in the HDPE plastic hydrocracking process. The process was carried out at 450°C for 2 hours with a flow of H_2 gas of 20 mL/minute with a feed /catalyst ratio = 5, the results shown in the data **Table 5**. Based on the data in **Table 5**, it can be seen that hydrocracking of HDPE plastic has occurred in all processes, which is characterized by the formation of hydrocracking products in 3 phases: liquid, solid, and gas with good conversion value (> 96%). The predominance of product gas (> 50%) for all processes carried out shows that the hydrocracking process takes place very hard, resulting in molecules that are too small in size and cannot be condensed with the cooling system used. Hydrocracking without a catalyst, better known as thermal cracking (pyrolysis), has been able to change HDPE plastic polymers, with the main product being the gas fraction. The hydrocracking process with the SiPILC catalyst is more exciting than thermal cracking, characterized by a decrease in liquid and solid products, which are converted to an increase in gas products. It is not expected because liquid products are less than optimal as the most expected products.

Table 5. The results of the hydrocracking process of HDPE plastic with thermal, SiPILC, and Ni/SiPILC catalysts with impregnated Ni variations

Catalyst	Hydrocracking products (%)			Conversion (%)
	Liquid	Solid	Gas	
Thermal	35.20	1.25	63.55	98.75
SiPILC	32.33	0.03	67.65	99.98
Ni 1%/SiPILC	42.48	2.09	55.44	97.92
Ni 2%/SiPILC	45.50	0.49	54.01	99.51
Ni 4%/SiPILC	45.24	3.20	51.56	96.80
Ni 6%/SiPILC	45.04	0.72	54.25	99.29
Ni 8%/SiPILC	43.69	2.15	54.16	97.85

Adding Ni metal to SiPILC has significantly increased the liquid product (> 31%). Combining the pore system in SiPILC and adding the metal catalyst Ni may synergistically lead to liquid products. Another fact is that adding Ni metal in SiPILC does not significantly affect the yield of liquid products, and other yield parameters tend to be constant. According to Lovás *et al*. [39], the chosen catalyst system strongly influences the total product distribution from polymer-catalyzed cracking processes. Besides the textural properties of the catalyst, the total acidity also plays a very significant role in the distribution of the final product. The acidity of the catalyst must be at a specific value for the catalyst to produce a satisfactory conversion. On the other hand, an acidity value that is too high can cause excessive cracking of the feed, so much loss of the liquid fraction evaporates into an unwanted gas product when liquid fuel products are preferred. However, because of obtaining liquid product and maximum conversion value, minimum solid product, and more efficient use of Ni sources, Ni 2%/SiPILC was chosen as the best variation. It is also consistent with the previous fact that the Ni 2%/SiPILC catalyst has the maximum acidity. Furthermore, to recognize the quality of liquid products as products with fuel characteristics, a characterization was carried out using GC-MS and compared with market pertalite type fuel, shown in **Fig. 11**. Based on the chromatogram in **Fig. 11**, it can be seen that all variations of HDPE plastic hydrocracking processes produce liquid products composed of molecules with a maximum retention time peak of up to 60 minutes. However, most of the relatively high-intensity peaks appear with a retention time of < 20 minutes, such as the peaks of the Pertalite fuel chromatogram. The formation of scattered peaks evidences the process of thermal cracking on HDPE plastic with a retention time of < 30 minutes. Hot at the temperature of 450 °C has been able to break most of the bonds in the HDPE plastic polymer so that it becomes smaller molecules and even gas products which reach 63.55% (**Table 5**). The pyrolysis process of HDPE plastic has been reported [37] using decalin solvent achieved the best selectivity to form olefins of 96.5% within 5 hours and a temperature of 375°C. Meanwhile, Gracida-Alvarez *et al*. [40] reported the pyrolysis of HDPE plastic waste by studying its secondary degradation through variations in temperature and steam residence time in a micro pyrolysis reactor. At a temperature of 625°C and a vapour residence time of 1.4 seconds, it produces a wide range of gas and liquid products, while at a temperature of 675°C and a vapour residence time of 5.6 seconds, it produces primarily gaseous hydrocarbons and poly aromatics. Kumar and Singh [41] reported the thermal degradation of HDPE plastic waste at temperatures of 400-550°C, where the liquid product increased with increasing processing time. FTIR and GC-MS analysis results of liquid products show the presence of hydrocarbons that make up gasoline, kerosene, and diesel. Based on **Fig. 11**, generally, the liquid product of the catalyzed hydrocracking process is dominated by the light fraction, which is indicated by the number of peaks with a retention time of < 10 minutes with a relatively higher intensity. Using SiPILC and Ni/SiPILC catalysts has increased the light fraction product, evident from the number of peaks with a retention time of < 10 minutes which is more than the thermal hydrocracking process. Another fact that can be seen from **Fig. 11** is that the addition of Ni metal at low variations (1 and 2%) was able to cut molecules with a retention time of >20 minutes. However, at a higher variation, it produced larger molecules, indicating the appearance of peaks, with a retention time > 20 minutes. The formation of these larger molecules is undoubtedly undesirable because it will interfere with and reduce the quality of the liquid product towards the type of fuel referred to as pertalite. If pertalite fuel is included in the gasoline fraction, the higher molecules will be included in the kerosene and diesel fuel. Based on the maximum liquid product recovery data in **Table 5**, the chromatogram of **Fig. 11**, the efficiency of using Ni metal, and the process with variations of Ni 2%/SiPILC catalyst are selected as the catalyst with the best performance.

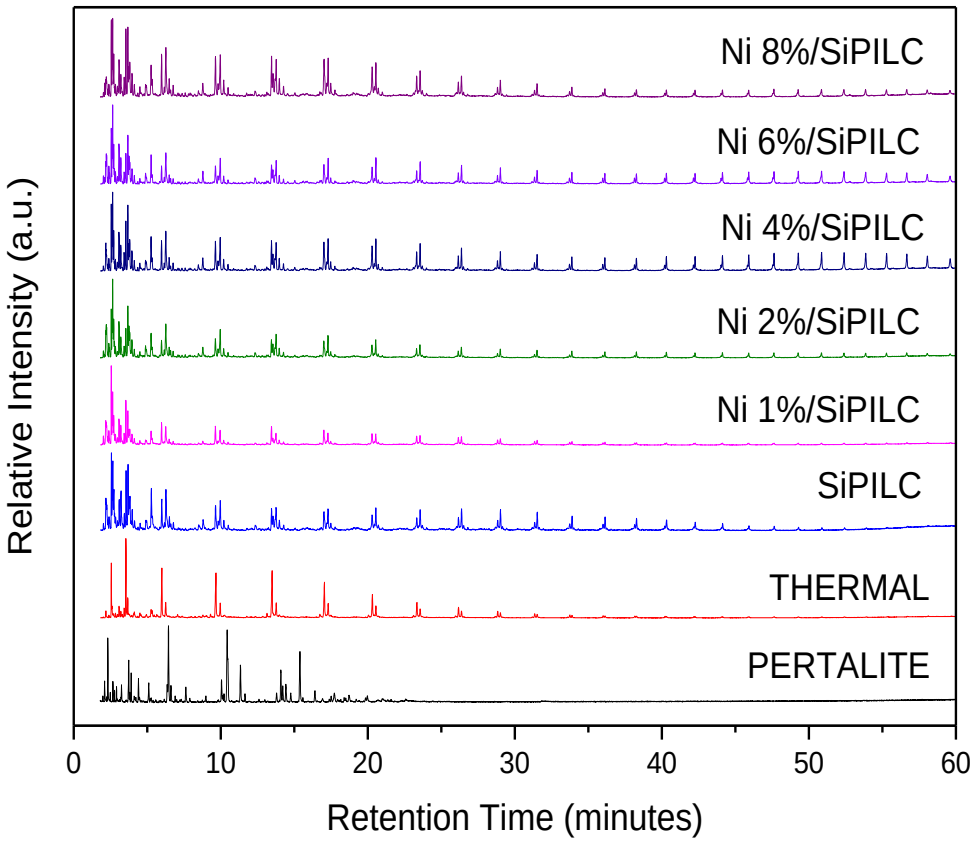

Fig. 11. Chromatogram of pertalite type market fuel and liquid products resulting from HDPE plastic hydrocracking at 450°C for 2 hours

3.4. Study of the hydrocracking temperature of HDPE plastic with Ni 2%/SiPILC catalyst

One of the essential factors determining the success of the plastic hydrocracking process by thermal pyrolysis or catalyzed pyrolysis is temperature. Therefore, a study of the hydrocracking temperature of HDPE plastic with Ni 2%/SiPILC catalyst was carried out, shown in **Table 6**. In this study, the temperature variation started at 450°C. The HDPE plastic had not turned into a gaseous fraction at the previous temperature, so it could not flow past the catalyst and into the condenser. Based on the data in **Table 6**, information was obtained that the higher the hydrocracking temperature, the more intense the breaking process of the polymer molecules making up HDPE plastic. Higher temperatures allow the plastic polymer molecules to be cut repeatedly so that they become molecules too small in size and become gaseous products. It is evidenced by the tendency of liquid products to decrease; conversely, gas products tend to increase with increasing temperature. The temperature of 450°C was chosen as the best temperature to get the most optimal liquid product. The hydrocracking process of HDPE plastic with a Fluid Catalytic Cracking (FCC) catalyst produces a maximum liquid product at a temperature of 450 °C which was also reported [11] by producing 91.2% liquid product, 4.1% gas product, and 4.7% coke. The yield of liquid products, which was far more than that obtained in this study, was probably due to the different types of catalysts where FCC is a commercial catalyst that has proven excellent selectivity to form molecules with sizes fulfilling the range of liquid products. According to Lovás *et al.* [36], the chosen catalyst system strongly influences the total product distribution from polymer-catalyzed cracking processes. Sriningsih *et al.* [19] dispersed Ni on natural zeolite to catalyze the cracking process of LDPE plastic waste to produce liquid fuel. The cracking process was carried out at 450°C for 1 hour to produce 30.64% liquid product, 68.27% gas product, and 1.10% solid product (coke). Lovás *et al.* [39] carried out the hydrocracking process of HDPE and PP plastic waste with an FCC catalyst at a temperature of 525°C to produce light gas fractions, LPG, gasoline fractions, and light and heavy vehicle oils. Meanwhile, John *et al.* [5] stated that if more liquid fuel yields are desired in plastic cracking, then a relatively low-temperature process (< 550°C) should be applied. An increased operating temperature will increase gas production and decrease the liquid product.

Table 6. HDPE plastic hydrocracking products with Ni 2%/SiPILC catalyst with temperature variations.

Temperature (°C)	Hydrocracking products (%)			Conversion (%)
	Liquid	Solid	Gas	
450	45.100	0.489	54.411	99.511
475	33.044	0.675	65.281	98.325
500	29.570	0.015	70.415	99.985

According to Artetxe *et al*. [42], HDPE plastic cracking was carried out in 2 stages: thermal cracking at a temperature of 500°C followed by HZSM-5 catalyzed cracking at a temperature of 350-550°C. The increase in temperature and the processing time increased the resulting light olefins reaching 62.9% at 550°C with a composition of 10.6% ethylene, 35.6% propylene, and 16.7% butene. Although the yield of single-ring aromatics increased with temperature and processing time, the maximum yield was lower than 13%. The difference in the distribution of polymer hydrocracking products, including plastics, is greatly influenced by the catalyst system chosen [39].

The performance of the Ni 2%/SiPILC catalyst in the process of hydrocracking HDPE plastics in producing liquid products (45.1 wt%, data **Table 6**) is still relatively low when compared to the results of relevant research, as shown in **Table 7**, especially against commercial synthetic catalysts such as FCC and ZSM-5 which are well known for their excellent performance. Apart from the main factors of catalyst type and temperature, there are many determining factors for the success of the plastic cracking process into liquid products.

3.5. Study of hydrocracking time optimization of HDPE plastic with Ni 2%/SiPILC catalyst

The cracking process always requires heat, so it involves an energy source. In order to determine the sufficient time effectively for the hydrocracking process of HDPE plastic with the best catalyst Ni 2%/SiPILC, a long hydrocracking study was carried out with variations: 0.5; 1; 1.5, and 2 hours to avoid wasting time and energy. The results of this review process are given in **Table 8**.

Based on the data in **Table 8**, it can be seen that with increasing hydrocracking time, the catalytic activity increases, which is indicated by an increase in a liquid product, a decrease in a solid product, and an increase in conversion value. The hydrocracking time was too long (2 hours). Even though it further reduced the solid product, it tended to reduce the liquid product and was converted to gas. Based on the optimal liquid product, energy efficiency, and time, the hydrocracking time variation of 1.5 hours was chosen as the best variation of length of time. Hydrocracking HDPE plastic with Ni/HSiAl catalyst at a temperature of 375°C, 1000 psi of H_2 gas for 1 hour produces a liquid comparable to premium gasoline fuel [44].

Table 7. Comparison of catalyst performance from several other relevant researchers in the processing of cracking HDPE plastics into liquid products

Catalyst	Temperature (ºC)	Liquid product (wt%)	Ref.
FCC	450	91.2	11
MCM-41	430	42.3	6
Bentonite Clay	500	82.5	43
ZSM-5	525	61.05	24
Ni 2%/SiPILC	450	45.1	This research

Table 8. Results of optimizing the length of time for the hydrocracking process of HDPE plastic with Ni 2%/SiPILC catalyst at 450°C.

Duration (hour)	Hydrocracking products (%)			Conversion (%)
	Liquid	Solid	Gas	
0.5	36.062	13.200	50.738	86.80
1	41.349	5.107	53.544	94.89
1.5	45.455	3.031	51.514	96.97
2	45.100	0.489	54.411	99.51

3.6. Composition of fractions in the liquid product resulting from the hydrocracking of HDPE plastic with Ni 2%/SiPILC catalyst

The composition of the fractions that make up the liquid product resulting from the hydrocracking of HDPE plastic and to determine the effect of using a catalyst can be calculated using the GC-MS data. The division of fractions by the number of C atomic ranges refers to Aguado *et al.* [24], which states that C_1-C_4 (gas), C_5-C_{12} (gasoline), C_{13}-C_{18} (light diesel), and C_{19}-C_{40} (heavy diesel). When paying attention to the popularity of gasoline and diesel fractions in the community, the range of gasoline (C_1-C_{12}) and diesel (C_{13}-C_{40}) is expanded, so the results of this study are shown in **Table 9**.

Based on the data in **Table 9**, all processes produce particular liquid products in the gasoline and diesel fractions with no different values. Using Ni 2%/SiPILC catalyst did not give a different effect in directing to a particular fraction. However, in **Table 5**, the previous Ni 2%/SiPILC catalyst led to a significant liquid product, from 35.20% (thermal process) to 45.50% (Ni 2%/SiPILC catalyzed process) with an increase of 10.30%. The catalytic cracking process for HDPE plastic has also been reported by Ghaffar *et al.* [24] used the ZSM-5 catalyst for 75 minutes with the highest oil yield of 61.05%, 0.41% solid product, and 38.54% gas product. The liquid product has the main component of C_{10}-C_{24} hydrocarbon compounds, the diesel fuel fraction.

Meanwhile, John *et al.* [4] reported the catalytic cracking process of HDPE plastic using the mineral potash catalyst with a catalyst/feed ratio = 30% (w/w), producing a liquid product of 34.7% with the main component being C_{11}-C_{20} hydrocarbon compounds which fall into the kerosene to petroleum fuel fraction range. The difference in these results is possible because many factors can affect the quantity and quality of liquid products resulting from cracking, one of which is using a different catalyst. The superiority of the Ni 2%/SiPILC catalyst compared to the ZSM-5 catalyst and the mineral potash is that it produces a light fraction included in the gasoline range, reaching 55.03% more in the liquid product. This data is more advantageous if it was looked at the gasoline fraction, which has a broader use, so it is relatively more valuable than the diesel fraction.

3.7. Reusability study of Ni 2%/SiPILC catalyst in HDPE plastic hydrocracking process

One of the superior properties of a catalyst is its ability to be used repeatedly (reusability). A reusability study was conducted to determine the reusability of the catalyst used in the same hydrocracking process using the new HDPE plastic feed. The results of this study will describe the catalyst's ability until its activity decreases so much that it needs to be regenerated. A reusability study was carried out for the catalyst with the best performance, Ni 2%/SiPILC, with an optimal hydrocracking time of 1.5 hours for five repetitions with each hydrocracking process using the new HDPE plastic feed. Data from the reusability study results are given in **Table 10**.

Based on the data in **Table 10**, it can be seen that the Ni 2%/SiPILC catalyst is capable of having a minimum catalytic activity of up to 5 repetitions in the HDPE plastic hydrocracking process, which is indicated by a suitable conversion value (> 94%) and the formation of liquid and gaseous products. The more frequent use of the Ni 2%/SiPILC catalyst shows a decreasing activity, as evidenced by the decreasing amount of liquid product and conversion. The decrease in activity was probably caused by the formation of coke as a solid product which increased with the more frequent use of the catalyst, from 0.49% to 5.10%. The coke formation allows the covering of the active side of the catalyst, thereby preventing direct contact with the plastic polymer feed molecules, resulting in the hampered hydrocracking process. The liquid product resulting from hydrocracking in the study of the reusability of the Ni 2%/SiPILC catalyst was then chosen to be characterized by GC-MS, whose chromatogram is presented in **Fig. 12**.

Table 9. Selectivity for the formation of gasoline and diesel fractions with various thermal processes, catalyzed by SiPILC and Ni 2%/SiPILC in the HDPE plastic hydrocracking process

Catalyst	Fraction selectivity in liquid products (%)	
	C_1-C_{12} (Gasoline)	C_{13}-C_{40} (Diesel)
Thermal	56.53	43.47
SiPILC	46.61	53.38
Ni 2%/SiPILC	55.03	44.96

Table 10. Data on reusability study of Ni 2% /SiPILC catalyst in HDPE plastic hydrocracking process, catalyst/feed ratio = 5, time 1.5 hours, temperature 450°C

Hydrocracking process	Hydrocracking products (%)			Conversion (%)
	Liquid	Solid accumulation	Gas	
1 (new)	45.10	0.49	54.41	99.51
2	42.43	0.78	56.79	99.22
3	43.20	2.79	54.01	97.21
4	43.26	3.75	52.99	96.25
5	41.08	5.10	53.82	94.90

Based on the chromatogram of **Fig. 12**, it can be seen that the use of a new catalyst, repeated three times and five times from Ni 2%/SiPILC catalyst in the HDPE plastic hydrocracking process produced a liquid product with the peaks of its constituent compounds mostly appearing with t_R < 20 minutes as possessed by Pertalite type fuel market. The three liquid products of the catalyzed process were dominated by light fraction compounds with t_R < 10 minutes. Based on the chromatogram patterns of the first and third processes, it was seen that there was an increase in the intensity of the peaks with t_R < 5 minutes. It indicated that the catalytic activity of Ni 2%/SiPILC was increasing. Furthermore, the chromatogram was used five times, and the chromatogram peaks started to decrease, which reflected a decrease in catalyst activity. It is probably due to the formation of more and more coke, as shown in **Table 9**, and the photo appearance of the liquid product in **Fig. 13**, which tends to get darker as the catalyst is used more frequently.

The formation of more coke will clog the pores and cover the active side of the catalyst so that its activity decreases and can even experience deactivation. According to Ibáñez *et al.* [45] reported that the HZSM-5-catalyzed HDPE plastic pyrolysis process for the formation of coke through 2 ways, which was: (i) initiation, which was the first hour of flow precisely in the entry from the catalyzed reactor, (ii) permanent coke formation, which was after the first hour the flow becomes more intense in the final position of the catalyzed reactor. The permanent coke formation step caused by light olefin condensation will lead to degradation of the microporous region and Bronsted acidity of the catalyst.

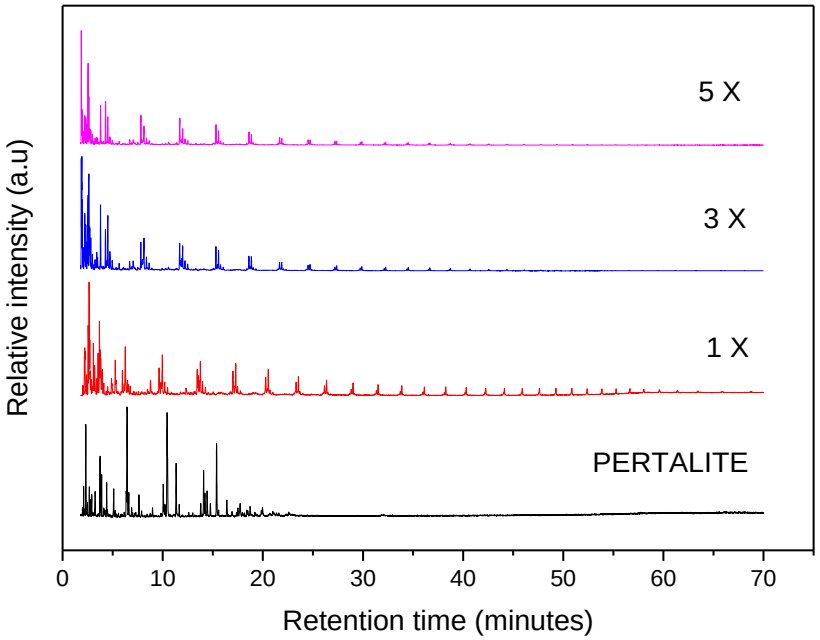

Fig. 12. Comparison of pertalite and liquid product chromatograms resulting from repeated HDPE plastic hydrocracking processes with Ni 2%/SiPILC catalyst

Fig. 13. Photo of a liquid product resulting from the hydrocracking of HDPE plastic with a Ni 2%/SiPILC catalyst with variations of catalyst reuse

The effect of catalyst reuse on catalyst quality is proven by XRD characterization for the used catalyst five times and the new catalyst, as shown in **Fig. 14**.

The breakdown of the solid structure of the catalyst may also cause coke formation. It was confirmed by the decreased peak intensity of d_{001} (at an angle of $2\theta = 4$-$5°$) on the diffractogram in **Fig. 14** after using the catalyst with five repetitions. It is probably due to the repeated use of heat, causing the long accumulation of heat treatment to become large, which allows damage to the pillar structure to begin. Starting the damage to the catalyst structure can also be proven by the SEM characterization of the new catalyst using the used catalyst five times, as shown in **Fig. 15**.

Based on the appearance of the SEM image in **Fig. 15**, it can be seen that the new (fresh) Ni 2%/SiPILC catalyst appears as a relatively uniform expanding material due to stretching material followed by the impregnation of Ni metal. Meanwhile, used Ni-2%/SiPILC catalyst, after five uses, are visible loss of the expanding globules present in the new catalyst and turning into random, disorganized flakes. Damage to the pillar structure may have begun. The presence of several white lumps in the two materials is probably the remaining Quartz mineral left over from the separation of clay initially into clay light fractions. It was confirmed from the peaks around the angle $2\theta = 26°$ in the diffractogram of the two materials, which are still clearly visible. Liu *et al.* [6] reported using a clay catalyst for cracking HDPE plastic, where the SEM results of the used clay catalyst changed from the initial clay structure, which was layered to agglomerate. The decrease in the activity of the Ni 2%/SiPILC catalyst after five uses can also be proven by measuring the Ni content in the fresh of Ni 2%/SiPILC and 2% Ni/SiPILC used five times the usage as presented in **Table 11**.

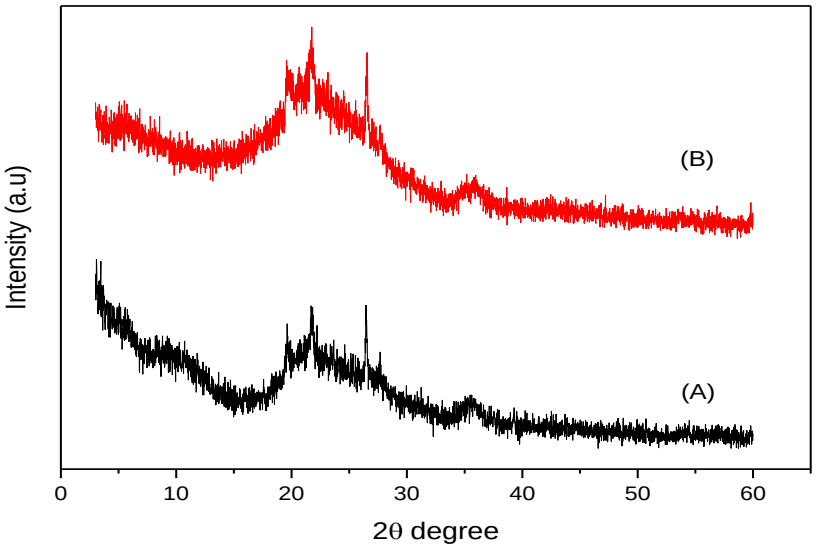

Fig. 14. The diffractogram of the new Ni 2%/SiPILC catalyst (A) and after using five times the HDPE plastic hydrocracking process (B)

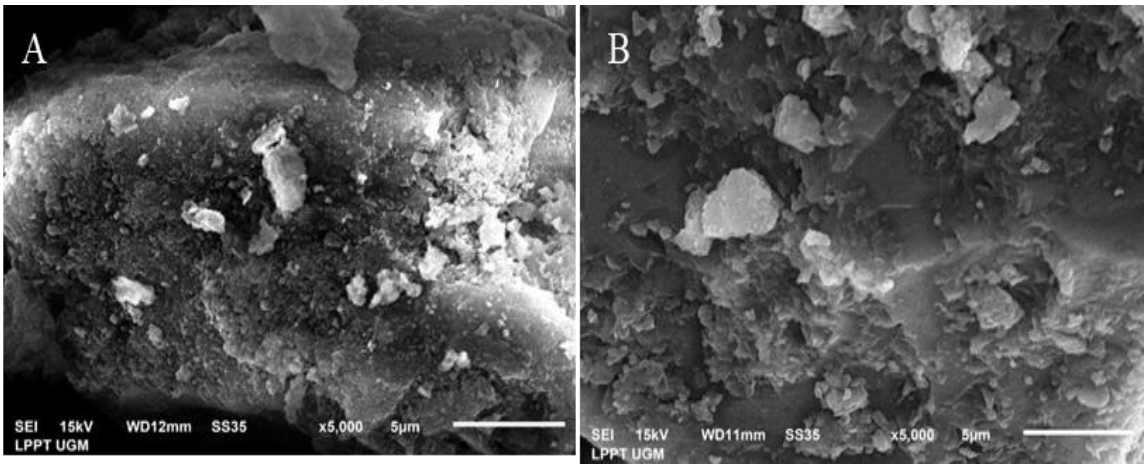

Fig. 15. SEM results of new Ni 2%/SiPILC catalyst (A) and Ni 2%/SiPILC after five uses (B) as catalysts in HDPE plastic hydrocracking process

Table 11. The metal content of Ni in fresh of Ni 2%/SiPILC and 2% Ni/SiPILC used

Sample	Content of Ni (mg/g)
Fresh Ni 2%/ SiPILC	272.15
Ni 2%/SiPILC used	67.44

Based on the data in **Table 11**, the content of Ni metal in the catalyst decreased drastically from 272.15 mg/g to 67.44 mg/g. This decrease can contribute to a decrease in the catalyst's performance, where the data in **Table 5** previously stated that adding Ni catalyst metal could increase the catalyst's performance. The decrease in catalyst activity can also be proven from the GSA analysis data where the specific surface area of the fresh Ni 2%/SiPILC catalyst is 431.72 m^2/g down to 210.74 m^2/g for used Ni 2%/SiPILC 5 times used. The decrease in specific surface area is consistent with previous data, which was the loss of the d_{001} peak on the diffractogram for 2% Ni 2%/SiPILC 5 times use (**Fig. 12**) and the loss of expanding material from SEM images (**Fig. 13**). This is the occurrence of damage to the pillar structure due to the effect of repeated heating. López *et al.* [43] also reported decreased spent catalyst activity López *et al.* [46] and stated that plastic waste catalyzed the ZSM-5 catalyst for cracking. The fresh ZSM-5 catalyst has a specific surface area of 412 m^2/g down to 291.6 m^2/g for the spent catalyst. The fresh ZSM-5 has a microporous surface area of 346.1 m^2/g, decreasing drastically to 3.0 m^2/g for the used catalyst and increasing the amount of coke attached to and covering the surface of ZSM-5 causing a decrease in ZSM-5's catalytic activity. Meanwhile, Kassargy *et al.* [47] reported that the repeated use of USY zeolite for polyethene-catalysed cracking of up to 14 repetitions had caused structural damage, as evidenced by a decrease in the typical peaks of USY zeolite in XRD data and a decrease in specific surface area from 700 m^2/g to 387 m^2/g.

4. Conclusions

Separation of the clay fraction resulted in a light fraction of 41.83% and a heavy fraction of 58.17%. Separation reduced the Quartz content from 87.54% in the initial clay to 28.67% for the clay light fraction. Ni/SiPILC catalyst can be synthesized from the clay light fraction. The best SiPILC-supporting solid was synthesized with a TEOS/clay mole ratio = 60 with a specific surface area parameter of 570.66 m^2/g. Optimum impregnation of Ni on SiPILC at 2% resulted in a Ni 2%/SiPILC catalyst with impregnated Ni of 272.15 mg/g, an acidity of 6.536 mmol/g. The best catalyst activity of Ni 2%/SiPILC in the HDPE plastic hydrocracking process at 450°C for 1.5 hours has a liquid product selectivity of 45.50%, with the selective liquid product leading to the gasoline fraction (55.03%) and diesel (44.96%). The reusability of Ni 2%/SiPILC catalyst with repeated use five times began to show a decrease in its catalytic activity due to structural damage, coke formation, and shrinkage of Ni metal content.

Acknowledgements

Thanks are conveyed to DRTPM Kemdikbudristek and LPPM Gadjah Mada University Yogyakarta for research funding support as stated in Master Contract Number: 089/E5/PG.02.00.PT/2022 and Derivative Contract Number: 1915/UN1/DITLIT/Dit-Lit/PT .01.03/2022.

References

[1] Lebreton, L., Andrady, A. Future scenarios of global plastic waste generation and disposal. *Palgrave Commun*, 5, (2019), 6.

[2] Prifti, K., Galeazzi, A. and Manenti, F., Design and Simulation of a Plastic Waste to Methanol Process Yield and Economics, *Ind. Eng. Chem. Res*, 62, (2023), 5083-5096,

[3] Mishra, R., Kumar, A., Singh, E. and Kumar, S., Recent Research Advancements in Catalytic Pyrolysis of Plastic Waste, *Sustainable Chem. Eng*. 11, (2023), 2033-2049.

[4] Ong, H.M., Veksha, A., Manh Ha, Q.L., Huang, J., Tsakadze, Z., and Lisak, G., Catalytic Activity and Coke resistance of Gasification Slag-Supported Ni Catalyst during Steam Reforming of Plastic Pyrolysis Gas, *Sustainable Chem. Eng*., 10, (2022), 17167-17176.

[5] John, D., Chukwuneke, C. E., Onuigbo, I. O., Yahaya, M. F., Agboola, B. O., Jahng, W. J. Low-temperature synthesis of kerosene- and diesel-range fuels from waste plastics using natural potash catalyst. *Inter. J. Energy Environ. Eng.*, 12 (3) (2021), 531-541.

[6] Liu, M., Zhuo, J. K., Xiong, S. J., Yao, Q. Catalytic Degradation of High-Density Polyethylene over a Clay Catalyst Compared with Other Catalysts. *Energy & Fuels*, 28 (9) (2014), 6038-6045.

[7] Ashworth, D. C., Elliott, P., Toledano, M. B. Waste incineration and adverse birth and neonatal outcomes: a systematic review. *Environ. Inter*., 69 (2014), 120-132.

[8] Dobo, Z., Kecsmar, G., Nagy, G., Koos, T., Muranszky, G. and Ayari, M., Characterization of Gasoline-like Transportation Fuels Obtained by Distillation of Pyrolysis Oils from Plastic Waste Mixtures, *Energy & Fuels*, 35, (2021), 2347-2356

[9] Din, M. I., Sadaf, S., Hussain, Z., Khalid, R. Assembly of superparamagnetic iron oxide nanoparticles (Fe3O4-Nps) for catalytic pyrolysis of corn cob biomass. *Energy Sources, Part A: Recovery, Utilization, and Environmental Effects*: (2020), 1-9.

[10] Borsodi, N., Miskolczi, N., Angyal, A., Bartha, L., Kohán, J., Lengyel, A., (2011), Hydrocarbons obtained by pyrolysis of contaminated waste plastics, *45th International Petroleum Conference, Bratislava, Slovak Republic*

[11] Abbas-Abadi, M. S., Haghighi, M. N., Yeganeh, H. Evaluation of pyrolysis product of virgin high-density polyethene degradation using different process parameters in a stirred reactor. *Fuel Processing Tech.*, 109 (2013), 90-95.

[12] Manos, G., Garforth, A., Dwyer, J. (Catalytic Degradation of High-Density Polyethylene on an Ultrastable-Y Zeolite. Nature of Initial Polymer Reactions, Pattern of Formation of Gas and Liquid Products, and Temperature Effects. *Indust. Eng. Chem. Res.*, 39 (5) (2000), 1203-1208.

[13] Farajfaed, S., Sharifian, S., Asasian-Kolur, N., Sillanpää, M. Granular silica pillared clay for levofloxacin and gemifloxacin adsorption from aqueous systems. *J. Environ. Chem. Eng.*, 9 (5) (2021), 106306.

[14] Li, B., Mao, H., Li, X., Ma, W., Liu, Z. Synthesis of mesoporous silica-pillared clay by intragallery ammonia-catalyzed hydrolysis of tetraethoxysilane using quaternary ammonium surfactants as gallery templates. *J. Colloid Interface Sci.*, 336 (1): (2009) 244-249.

[15] Dincer, B. Y., Balcı, S., Tomul, F. In-situ mesoporous silica pillared clay synthesis and titanium and iron incorporation effect on structural properties. *Micropor. Mesopor. Mater.*, 305 (2020), 110342.

[16] Han, Y.-S., Matsumoto, H., Yamanaka, S. Preparation of New Silica Sol-Based Pillared Clays with High Surface Area and High Thermal Stability. *Chem. Mater.*, 9 (9): (1997), 2013-2018.

[17] Zhou, C., Li, X., Ge, Z., Li, Q., Tong, D. Synthesis and acid catalysis of nanoporous silica/alumina-clay composites. *Catalysis Today*, 93-95: (2004), 607-613.

[18] Chmielarz, L., Gil, B., Kuśtrowski, P., Piwowarska, Z., Dudek, B., Michalik, M. Montmorillonite-based porous clay heterostructures (PCHs) intercalated with silica–titania pillars—synthesis and characterization. *J. Solid State Chem.*, 182 (5) (2009), 1094-1104.

[19] Sriningsih, W., Saerodji, M. G., Trisunaryanti, W., Triyono, Armunanto, R., Falah, I. I. Fuel Production from LDPE Plastic Waste over Natural Zeolite Supported Ni, Ni-Mo, Co and Co-Mo Metals. *Procedia Environ. Sci.*, 20 (2014), 215-224.

[20] Yao, D., Yang, H., Chen, H., Williams, P. T. Co-precipitation, impregnation and so-gel preparation of Ni catalysts for pyrolysis-catalytic steam reforming of waste plastics. *Appl. Catal. B: Environ*, 239 (2018), 565-577.

[21] Qureshi, M.S., Nisar, S., Shah, R. And Salman, H., , Studies of Liquid Fuel Formation from Plastic Waste by Catalytic Cracking Over Modified Natural Clay and Nickel Nanoparticles, sci.Ind. res. Ser. A: Phys sci. 63A, (2020), 79-88

[22] Al-asadi, M., Miskolczi, N. Pyrolysis of polyethylene terephthalate containing real waste plastics using Ni loaded zeolite catalysts. *IOP Conference Series: Earth and Environmental Science*, 154 (1) (2018), 012021.

[23] Mangesh, V. L., Perumal, T., Subramanian, S., Padmanabhan, S. Clean Energy from Plastic: Production of Hydroprocessed Waste Polypropylene Pyrolysis Oil Utilizing a Ni–Mo/Laponite Catalyst. *Energy & Fuels*, 34 (7) (2020), 8824-8836.

[24] Ghaffar, N. F. A., Johari, A., Abdullah, T. A. T., Ripin, A. Catalytic Cracking of High-Density Polyethylene Pyrolysis Vapor over Zeolite ZSM-5 Towards Production of Diesel. *IOP Conference Series: Mater. Sci. Eng.*, 808 (1) (2020), 012025.

[25] Geramian, M., Osacky, M., Ivey, D.G., Liu, Q. And Etsell, T.H., Effect of Swelling Clay Minerals (Montmorillonite and Illite-Smectite) on Nonaqueous Bitumen Extraction from Alberta Oil Sands, *Energy & Fuels*, 30, (2016), 8083-8090.

[26] Barakan and Aghazadeh, synthesis and characterization of hierarchical porous clay heterostructure from Al, Fe-pillared nano bentonite using microwave and ultrasonic techniques, *Micropor. Mesopor. Mater*, 278, (2019), 138-148.

[27] Mao, H., Liu, X., Yang, J., Li, B., Chen, Q., Zhong, J. Fabrication of magnetic silica-pillared clay (SPC) nanocomposites with ordered interlayer mesoporous structure for controlled drug release. *Micropor. Mesopor. Mater*, 184 (2014), 169-176.

[28] Alandis, N. M., Mekhamer, W., Aldayel, O., Hefne, J. A. A., Alam, M. Adsorptive Applications of Montmorillonite Clay for the Removal of Ag(I) and Cu(II) from Aqueous Medium. *J. Chem.*, 2019 (2019), 7129014.

[29] Ren, Z., Zhang, F., Yue, L., Li, X., Tao, Y., Zhang, G., Wu, K., Wang, C., Li, B. Nickel nanoparticles highly dispersed in pillared silica clay as an efficient catalyst for chlorobenzene dechlorination. *RSC Adv.*, 5 (65): (2015), 52658-52666.

[30] Asgari, M., Vitale, G., Sundararaj, U. Synthesis and characterization of a novel nickel pillared–clay catalyst: In-situ carbon nanotube–clay hybrid nanofiller from Ni-PILC. *Appl. Clay Sci.*, 205 (2021), 106064.

[31] Mao, H., Li, B., Yue, L., Wang, L., Yang, J., Gao, X. Aluminated mesoporous silica-pillared montmorillonite as acidic catalyst for catalytic cracking. *Appl. Clay Sci.*, 53 (4) (2011), 676-683.

[32] Richardson, J. T., Scates, R., Twigg, M. V. X-ray diffraction study of nickel oxide reduction by hydrogen. *Appl. Catal. A: General*, 246 (1) (2003), 137-150.

[33] Aguado, J., Serrano, D. P., Escola, J. M., Briones, L. Deactivation and regeneration of a Ni supported hierarchical Beta zeolite catalyst used in the hydroreforming of the oil produced by LDPE thermal cracking. *Fuel*, 109 (2013), 679-686.

[34] Garrone, E., Fajula, F., Acidity and Basicity of Ordered Silica-based Mesoporous Materials, in *Acidity and Basicity*, Springer Berlin Heidelberg, Berlin, Heidelberg, (2008).

[35] Jystad, A., Leblanc, H., Caricato, M. Surface Acidity Characterization of Metal-Doped Amorphous Silicates via Py-FTIR and 15N NMR Simulations. *J. Physic. Chem. C*, 124 (28) (2020), 15231-15240.

[36] Eleeza, J., Boahene, P., Vedachalam, S., Dalai, A. K., Adjaye, J. Influence of Catalyst Acidity on Fine Particle Deposition during Hydrotreating of Bitumen-Derived Heavy Gas Oil. *Energy & Fuels*, 35 (20) (2021), 16735-16749.

[37] Sekewael, S. J., Wijaya, K., Triyono, T. Chemical modification of Montmorillonite K10 and its catalytic activity. *Asian J. Chem.*, 32 (3) (2020), 659-664.

[38] Mao, H., Li, B., Li, X., Liu, Z., Ma, W. Mesoporous nickel-containing silica-pillared clays (Ni-SPC): Synthesis, characterization and catalytic behaviour for cracking of plant asphalt. *Catal. Commun*, 10 (6) (2009), 975-980.

[39] Lovás, P., Hudec, P., Jambor, B., Hájeková, E., Horňáček, M. Catalytic cracking of heavy fractions from the pyrolysis of waste HDPE and PP. *Fuel*, 203: (2017), 244-252.

[40] Gracida-Alvarez, U. R., Mitchell, M. K., Sacramento-Rivero, J. C., Shonnard, D. R. Effect of Temperature and Vapor Residence Time on the Micropyrolysis Products of Waste High-Density Polyethylene. *Indust. Eng. Chem. Res.*, 57 (6) (2018), 1912-1923.

[41] Kumar, S., Singh, R. Recovery of hydrocarbon liquid from waste high-density polyethylene by thermal pyrolysis. *Brazilian J. Chem. Eng.*, 28 (2011), 659-667.

[42] Artetxe, M., Lopez, G., Amutio, M., Elordi, G., Bilbao, J., Olazar, M. Light olefins from HDPE cracking in a two-step thermal and catalytic process. *Chem. Eng. J.*, 207-208 (2012), 27-34.

[43] Panda A.K., Thermo-catalytic degradation of different plastics to drop in liquid fuel using calcium bentonite catalyst, *Inter. J. Indust. Chem.*, 9, (2018), 167-176.

[44] Ding, W., Liang, J., Anderson, L. L. Hydrocracking and Hydroisomerization of High-Density Polyethylene and Waste Plastic over Zeolite and Silica−Alumina-

Supported Ni and Ni−Mo Sulfides. *Energy & Fuels*, 11 (6) (1997), 1219-1224.

[45] Ibáñez, M., Artetxe, M., Lopez, G., Elordi, G., Bilbao, J., Olazar, M., Castaño, P. Identification of the coke deposited on an HZSM-5 zeolite catalyst during the sequenced pyrolysis–cracking of HDPE. *Appl. Catal. B: Environ*, 148-149 (2014), 436-445.

[46] López, A., de Marco, I., Caballero, B. M., Adrados, A., Laresgoiti, M. F. Deactivation and regeneration of ZSM-5 zeolite in catalytic pyrolysis of plastic wastes. *Waste Management*, 31 (8) (2011), 1852-1858.

[47] Kassargy, C., Awad, S., Burnens, G., Upreti, G., Kahine, K., Tazerout, M. Study of the effects of regeneration of USY zeolite on the catalytic cracking of polyethylene. *Appl. Catal. B: Environ*, 244 (2019), 704-708.